Azimuthal correlations of pions in relativistic heavy-ion collisions at 1 GeV/nucleon

S. A. Bass,[1,2] C. Hartnack,[2,3] H. Stöcker,[1] and W. Greiner[1]

[1]Institut für Theoretische Physik der J. W. Goethe Universität, Postfach 11 19 32, D-60054 Frankfurt am Main, Germany
[2]Gesselschaft für Schwerionenforschung Darmstadt, Postfach 11 05 52, D-64220 Darmstadt, Germany
[3]Laboratoire de Physique Nucléaire, Nantes, France
(Received 3 January 1995)

Triple differential cross sections of pions in heavy-ion collisions at 1 GeV/nucleon are studied with the isospin quantum molecular dynamics (IQMD) model. After discussing general properties of Δ resonance and pion production we focus on azimuthal correlations: At projectile- and target-rapidities we observe an anticorrelation in the in-plane transverse momentum between pions and protons. At c.m.-rapidity, however, we find that high p_t pions are being preferentially emitted perpendicular to the event plane. We investigate the causes of those correlations and their sensitivity on the density and momentum dependence of the real and imaginary part of the nucleon and pion optical potential.

PACS number(s): 25.75.+r

I. INTRODUCTION

One of the main goals of the study of relativistic heavy-ion collisions is the determination of the density and momentum dependence of the real and imaginary parts of the nucleon (and other hadron) optical potential (often also termed nuclear equation of state) [1–7]. Its importance stretches well beyond nuclear physics and is of great importance for the formation of nuclear matter after the big bang, the behavior of supernovas and neutron stars. It also is important for the quest for the quark-gluon plasma in heavy-ion collisions.

An increasing number of observables which are accessible through heavy-ion collisions has been found to be sensitive to the equation of state: Among the most prominent ones are collective flow effects such as the bounce-off of cold spectator matter *in* the reaction plane [8] and the squeeze-out of hot and compressed participant matter *perpendicular* to the reaction plane [9] as well as particle production [10–12]. The pion multiplicity was one of the first observables suggested to be sensitive to the nuclear equation of state [10–12]. This motivated a strong experimental effort (4π analysis of streamer chamber events at the BEVALAC) [13–15]. However, the sensitivity of pion yields and spectra [16] on the equation of state is not very high [17,18] and therefore the attention shifted towards *subthreshold* production of mesons (e.g., kaons and η mesons) [19–23].

New experimental 4π setups at two of the major heavy-ion reasearch facilities, GSI (FOPI, KaoS, TAPS) and LBL (TPC), enable the investigation of the emission pattern and correlations of primary and secondary particles in a far more detailed manner than ever before. It is now for the first time possible to thoroughly investigate correlation phenomena such as in-plane bounce-off [24–27] and out-of-plane squeeze-out [28–30] of *pions*. The detailed investigation of these effects, including their possible origin and their impact parameter and p_t dependences as well as their sensitivity to the nuclear equation of state, is the subject of this paper.

II. ISOSPIN QUANTUM MOLECULAR DYNAMICS (IQMD) MODEL

The first widely used microscopic models for the description of relativistic heavy-ion collisions were based on Vlasov-Uehling-Uhlenbeck (VUU) theory [18,31,32], which explicitly treats nonequilibrium and (stochastic) quantum effects in the framework of one-particle quantities, as well as the nuclear potential (nuclear equation of state). The dynamical basis of the VUU model is the following transport equation:

$$\frac{\partial f}{\partial t} + \vec{v} \cdot \nabla_r f - \nabla_r U \cdot \nabla_p f$$

$$= -\frac{4}{(2\pi)^3} \int d^3 p_2 \, d^3 p'_2 \, d^3 p'_1 \, d\Omega \, v_{12} \frac{d\sigma}{d\Omega}$$
$$\times [f f_2 (1 - f'_1)(1 - f'_2) - f'_1 f'_2 (1 - f)(1 - f_2)]$$
$$\times \delta^3 (p + p_2 - p'_1 - p'_2).$$

f is the single-particle distribution function. The left-hand side (LHS) contains the potential U. Usually U is parametrized using the Skyrme ansatz. This gives us the opportunity to study the effects of the nuclear equation of state via different parameter sets.

The RHS contains the cross section σ and the Nordheim-Uehling-Uhlenbeck modifications incorporating the Pauli-blocking factors [33]. Models based on the same theory, but differing in numerical implementation, are the Boltzmann-Uehling-Uhlenbeck (BUU) [32] and the Landau-Vlasov [34] models. All three-dimensional (3D) numerical implementations of VUU theory are solved with the test particle method. The number of test particles used to represent a nucleon varies with the numerical implementation. The test particle method solves Hamilton's equation of motion for each test particle. These transport models have been successful in studying various aspects of relativistic heavy-ion colli-

S. A. BASS, C. HARTNACK, H. STÖCKER, AND W. GREINER

sions, such as single-particle spectra, collective effects (stopping, bounce-off, squeeze-out), and meson production.

However, certain fluctuations and correlations, such as the formation of fragments in relativistic heavy-ion collisions, cannot be studied with a transport model based on a single-particle distribution function. This was one of the motivations for the developement of the quantum molecular dynamics model (QMD) [21,35–37]. In the QMD model the baryons are represented by Gaussian-shaped density distributions

$$f_i(\vec{r}, \vec{p}, t) = \frac{1}{\pi^2 \hbar^2} e^{-[\vec{r}-\vec{r}_{i0}(t)]^2 \frac{1}{2L}} e^{-[\vec{p}-\vec{p}_{i0}(t)]^2 \frac{2L}{\hbar^2}} .$$

They are initialized in a sphere of a radius $R = 1.14 A^{1/3}$ fm, in accordance with the liquid drop model. Each nucleon occupies a volume of h^3, so that phase space is uniformly filled. The initial momenta are randomly chosen between 0 and the local Thomas-Fermi momentum. The A_P and A_T nucleons interact via two- and three-body Skyrme forces, a Yukawa potential, and momentum-dependent interactions. Subsequently, the fermionic molecular dynamics (FMD) [38], antisymmetrized molecular dynamics (AMD) [39], and quantum molecular dynamics with Pauli potential (PQMD) [40] models have been developed to offer an improved treatment of the Pauli principle.

Isospin is treated explicitly (in the so-called IQMD version); a symmetry potential (to achieve corrected distributions of protons and neutrons in the nucleus) and explicit Coulomb forces between the Z_P and Z_T protons are included.

Pion production is treated via the delta resonance [24,41,42]. A frozen Δ approximation (infinite lifetime for the Δ resonance) had been used in other versions of the QMD model.

The hadrons propagate under the influence of the potential in Hamilton's equations of motion:

$$\dot{p}_i = -\frac{\partial H}{\partial q_i}, \quad \dot{q}_i = \frac{\partial H}{\partial p_i} ,$$

with

$$H = T + V = \sum_i \frac{p_i^2}{2m_i} + \sum_i \sum_{j>i}$$

$$\times \int f_i(\vec{r}, \vec{p}, t) V^{ij} f_j(\vec{r}', \vec{p}', t) \, d\vec{r} \, d\vec{r}' \, d\vec{p} \, d\vec{p}' .$$

The baryon potential $V^{ij} = V_{\text{loc}}^{ij} + V_{\text{Yuk}}^{ij} + V_{\text{Coul}}^{ij} + V_{\text{mdi}}^{ij} + V_{\text{sym}}^{ij}$ consists of

$$V_{\text{loc}}^{ij} = t_1 \delta(\vec{r}_i - \vec{r}_j) + \sum_{k>j>i} \int f_k(\vec{r}'', \vec{p}'') t_2 \delta(\vec{r}_i - \vec{r}_j)$$

$$\times \delta(\vec{r}_i - \vec{r}_k) d\vec{r}'' d\vec{p}'' ,$$

$$V_{\text{Yuk}}^{ij} = t_3 \frac{\exp\{|\vec{r}_i - \vec{r}_j|/\mu\}}{|\vec{r}_i - \vec{r}_j|/\mu} ,$$

$$V_{\text{Coul}}^{ij} = \frac{Z_i Z_j e^2}{|\vec{r}_i - \vec{r}_j|} ,$$

$$V_{\text{mdi}}^{ij} = t_4 \ln^2[1 + t_5(\vec{p}_i - \vec{p}_j)^2] \delta(\vec{r}_i - \vec{r}_j) ,$$

$$V_{\text{sym}}^{ij} = t_6 \frac{1}{\varrho_0} T_{3i} T_{3j} \delta(\vec{r}_i - \vec{r}_j) .$$

The three-body term in V_{loc}^{ij} as stated above is only valid for a hard equation of state (for a soft equation of state a VUU-type formulation $\sim \rho^\gamma$ has to be used); Z_i, Z_j denote the charges of the baryons i and j, and T_{3i}, T_{3j} are their respective T_3 components. The meson potential only consists of the Coulomb potential.

The parameters μ and $t_1, ..., t_6$ are adjusted to the real part of the nucleon optical potential. For the density dependence of the nucleon optical potential standard Skyrme-type parametrizations are used. Two different equations of state have been implemented: a hard equation of state (H) with a compressibility of 380 MeV and a soft equation of state (S) with a compressibility of 200 MeV [18,31]. A fit of the momentum dependence to measurements [43,44] of the real part of the nucleon optical potential [6,21,45] yields

$$\delta \ln^2 \left[\varepsilon \cdot (\Delta \vec{p})^2 + 1 \right] \left(\frac{\rho}{\rho_0} \right) .$$

The equation of state (EOS) in its standard Skyrme-type parametrization including momentum dependence then reads

$$U = \alpha \left(\frac{\rho}{\rho_0} \right) + \beta \left(\frac{\rho}{\rho_0} \right)^\gamma + \delta \ln^2 \left[\varepsilon (\Delta \vec{p})^2 + 1 \right] \left(\frac{\rho}{\rho_0} \right) .$$

The mean field notation with the parameters α, β, γ, δ, and ϵ has been chosen for reasons of simplicity and in order to compare the parameters with those used in VUU-BUU calculations. Their values can be found in Table I. While the forces are calculated via the nucleon density in VUU-BUU calculations, a sum over two-particle interactions is performed in QMD-IQMD calculations.

The parameters $t_1, ..., t_6$ are calculated in the IQMD model before the initialization of the projectile and target nuclei from the tabulated values of α, β, γ, δ, and ϵ which serve as input. The width and normalization of the Gaussian wave packets have to be taken into account for the proper determination of the force parameters.

Hard N-N collisions are included by employing the collision term of the well-known VUU-BUU equation [4,18,32,46,47]. The collisions are done stochastically, in a similar way as in the cascade models [48,49]. Two particles collide if their minimum distance d fulfills

$$d \leq d_0 = \sqrt{\frac{\sigma_{\text{tot}}}{\pi}}, \qquad \sigma_{\text{tot}} = \sigma(\sqrt{s}, \text{type}),$$

"type" denotes the ingoing collision partners ($N-N, N-\Delta, N-\pi, ...$). In addition, the Pauli blocking (of the final state) of baryons is taken into account by checking the phase space densities in the final states of a two-body collision. The final phase space fractions P_1 and P_2 which are already occupied by other nucleons are determined for each of the two scattering baryons. The particular attempt for a collision is then blocked with the probability

$$P_{\text{block}} = 1 - (1 - P_1)(1 - P_2) .$$

TABLE I. Parameter sets for the nuclear equation of state used in the IQMD model. S and H refer to the soft and hard equations of state; M refers to the inclusion of the momentum-dependent interaction.

	α (MeV)	β (MeV)	γ	δ (MeV)	$\varepsilon \left(\frac{c^2}{\text{GeV}^2}\right)$
S	−356	303	1.17		
SM	−390	320	1.14	1.57	500
H	−124	71	2.00		
HM	−130	59	2.09	1.57	500

Whenever an attempted collision is blocked the scattering partners maintain the original momenta prior to scattering. Delta decays are checked in an analogous fashion with respect to the phase space of the resulting nucleon.

Pions are formed in the IQMD model via the decay of the delta resonance. The following inelastic reactions are explicitly taken into account and constitute the imaginary part of the pion optical potential, which is dominant in the 1 GeV/u energy domain [50]:

$$
\begin{aligned}
&\text{(a)} \quad NN \;\rightarrow\; \Delta N \quad &&\text{(hard-delta production)}\,, \\
&\text{(b)} \quad \Delta \;\rightarrow\; N\pi \quad &&(\Delta \text{ decay})\,, \\
&\text{(c)} \quad \Delta N \;\rightarrow\; NN \quad &&(\Delta \text{ absorption})\,, \\
&\text{(d)} \quad N\pi \;\rightarrow\; \Delta \quad &&\text{(soft-delta production)}\,.
\end{aligned}
$$

Elastic $\pi - \pi$, $\pi - N$, $\pi - \Delta$, $\Delta - \Delta$, $\Delta - N$ scattering is not taken into account. Experimental cross sections are used for processes (a) and (d) [51], as well as for the elastic N-N collisions. The respective cross sections are shown in Fig. 1.

For the delta absorption, process (c), we use a modified detailed balance formula [52]. The conventional detailed balance formula is only correct for particles with infinite lifetimes (zero width). If the principle of detailed balance is applied to the delta resonance, then its finite width has to be taken into account:

$$
\frac{d\sigma^{N\Delta \rightarrow NN}}{d\Omega} = \frac{1}{4} \frac{m_\Delta p_{NN}^2}{p_{N\Delta}} \frac{d\sigma^{NN \rightarrow N\Delta}}{d\Omega} \left(\frac{1}{2\pi} \int_{m_N + m_\pi}^{\sqrt{s} - m_N} p_{N\Delta} A_r(M) 2M \, dM \right)^{-1} ,
$$

with

$$
A_r(M) = \frac{\Gamma/2}{(M - m_\Delta)^2 + (\Gamma/2)^2} .
$$

The mass-dependent Δ-decay width has been taken from [53]

$$
\Gamma_\Delta(p_\pi) = \frac{r(p_\pi)}{r(p_0)} \Gamma_0
$$

with

$$
r(p) = \frac{p^3}{1 + \left(\frac{p}{p_1}\right)^2 + \left(\frac{p}{p_1}\right)^4} .
$$

p_π is the decay momentum of the pion, $p_0 = 227$ MeV/c, $p_1 = 238$ MeV/c, $p_2 = 318$ MeV/c and $\Gamma_0 = 120$ MeV. The Δ decays isotropically in its rest frame.

The elastic nucleon-nucleon scattering angular distribution is taken to be [54]

$$
\frac{d\sigma_{\text{el}}}{d\Omega} \sim \exp[A(s)\, t] ,
$$

where t is $-q^2$, the squared momentum transfer and

$$
A(s) = 6 \frac{[3.65\,(\sqrt{s} - 1.8766)]^6}{1 + [3.65\,(\sqrt{s} - 1.8766)]^6} .
$$

$\sqrt{s}$ is the c.m. energy in GeV and A is given in $(\text{GeV}/c)^{-2}$.

The inealstic channel is treated in an analogous fash-ion. The parametrization suggested by Huber and Aichelin [55] is used: fitted differential cross sections are extracted from one-boson-exchange (OBE) calculations:

$$
\frac{d\sigma_{\text{in}}}{d\Omega} \sim a(s)\, \exp[b(s)\, \cos\theta] .
$$

$a(s)$ and $b(s)$ are functions of $\sqrt{s}$ and vary in their definition for different intervals of $\sqrt{s}$ (see Table II).

Pions propagate between collisions (imaginary part of the pion optical potential) on curved trajectories with Coulomb forces acting upon them. The different isospin channels are taken into account using the respective Clebsch-Gordan coefficients

$$
\begin{aligned}
\Delta^{++} &\rightarrow 1(p + \pi^+), \quad \Delta^+ \rightarrow \tfrac{2}{3}(p + \pi^0) + \tfrac{1}{3}(n + \pi^+), \\
\Delta^0 &\rightarrow \tfrac{2}{3}(n + \pi^0) + \tfrac{1}{3}(p + \pi^-), \quad \Delta^- \rightarrow 1(n + \pi^-).
\end{aligned}
$$

The real part of the pion optical potential is treated in the following manner: As far as the pion is bound in a Δ resonance, the density- and momentum-dependent real part of the nucleon optical potential is applied as an approximation to the (yet unknown) real part of the Δ optical potential. Because of the large π-N cross section, intermediate pions are quite frequently bound in a delta resonance and in that interval the real part of the pion optical potential is substituted by the real part of the Δ optical potential. Free intermediate and final charged pions experience Coulomb forces which contribute to the real part of the pion optical potential. Recent investigations on the influence of the nuclear medium correction to the dispersion relation of the free pion have shown

TABLE II. $a(s)$ and $b(s)$ as functions of the c.m. energy.

$x = \sqrt{s}$ (GeV)	a (fm)	b
2.104 – 2.12	$294.6\ (x - 2.014)^{2.578}$	$19.71\ (x - 2.014)^{1.551}$
2.12 – 2.43	$\frac{0.01224}{(x-2.225)^2 + 0.004112}$	$19.71\ (x - 2.014)^{1.551}$
2.43 – 4.50	$(2.343/x)^{43.17}$	$33.41\ \arctan(0.5404\ (x - 2.146)^{0.9784})$

conflicting results [56,57] with respect to the importance of the modification for low-momentum pions. However, both calculations show that the high-energy part of the pion spectrum remains unchanged by this modification. Since our results are mainly for this high-energy contribution, we omit this medium correction, until a consensus has been achieved on the proper form of the respective medium contribution.

After a pion is produced (be it free or *bound* in a delta), its fate is governed by two distinct processes:
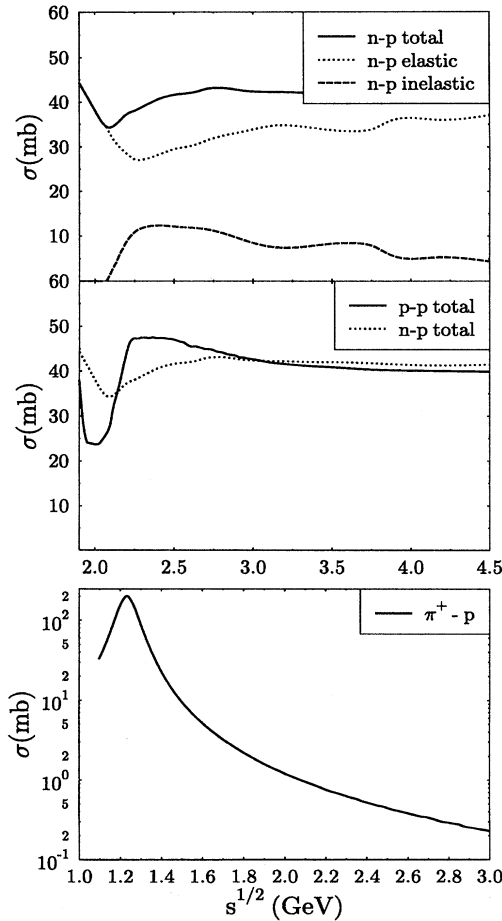

FIG. 1. Tabulated cross sections in the IQMD model. The upper frame shows the total, elastic, and inelastic proton neutron cross section. The middle frame compares the total proton neutron with the total proton proton cross section and the lower frame shows the total π^+ proton (or π^- neutron) cross section. The other pion nucleon cross sections are determined by scaling the π^+ proton cross section either with $1/3$ (π^+ neutron and π^- proton) or with $2/3$ (π^0 neutron and π^0 proton).

(1) absorption $\pi N N \to \Delta N \to N N$,
(2) scattering (resorption) $\pi N \to \Delta \to \pi N$.
In the CASCADE mode all real forces are turned off: Nucleons, pions, and deltas are propagated on straight lines between collisions.

III. FORMATION AND SPECTROSCOPY OF Δ RESONANCE MATTER

Recently an old subtopic [10,58] of this research has received renewed attention [59–63]: the possibility of producing Δ matter (or, in more general terms, *resonance matter*). At beam energies above a few hundred MeV/nucleon, the nucleons can be excited into Δ resonances. If the density of these resonances is as high as the nuclear matter ground state density, then a new state of matter, Δ matter, has been created. One of the potential signals for the presence of Δ matter is the creation of pions as decay products of the Δ resonance.

How can Δ matter be produced? Figure 2 shows the pion-nucleon cycle in the IQMD model. The scheme describes (for impact parameters $b \leq 5$ fm and averaged over 60 fm/c) possible processes linked to the creation of Δ matter. The probabilities in the boxes always refer to the vertices they are directly connected with. Δ resonances are initially produced via inelastic nucleon nucleon scattering. The produced resonances can either be reabsorbed via inelastic scattering or decay by emitting a pion. The pion can then either *freeze out* or interact with a nucleon to form a Δ again. In case the Δ has been absorbed the corresponding high-energetic ergetic nucleon might have a second chance of becoming a Δ by inelastic scattering. It could also transfer energy via elastic scattering onto another nucleon which then could scatter inelastically and form a new Δ. A nucleon interacts on the average about 3 times before it freezes out. This value fluctuates considerably, depending on whether the nucleon was in the participant zone (geometrical overlap of the colliding heavy ions) or in the spectator zone of the collision.

Unfortunately, the probablity for a nucleon to undergo inelastic scattering and to form a Δ during the heavy-ion collision is as low as 10%. The main process for sustaining Δ matter is the $\Delta \to N\pi \to \Delta$ loop, which, however, first has to be fueled by the $NN \to \Delta N$ process. The average pion passes approximately 3 times through this loop (it has been created by the decay of a *hard* Δ). However, 30% pass more than 6 times through the loop. For nucleons the probability of forming a *soft* Δ, i.e., via $\pi N \to \Delta$, is almost twice as high (Δ-*matter pump*) than the probability of forming a *hard* Δ via $NN \to N\Delta$.

Figure 3(a) shows the time evolution of the total

baryon, nucleon, and Δ densities in units of ρ/ρ_0 (top). The densities are calculated in a sphere of 2 fm radius around the collision center. Between 5 fm/c and 20 fm/c more than 20 Δ resonances can be found in the system: This time interval coincides with the hot and dense reaction phase. At 10 fm/c up to 55 resonances are present in the *total* reaction volume (keep in mind this is *not* in the 2 fm test sphere). A Δ multiplicity of > 40 can be sustained for an interval of 10 fm/c, 6 times longer than the lifetime of a free Δ resonance. However, this is not pure Δ matter: In the small *test* volume shown in Fig. 2(a) the resonance *density* is $0.5\rho_0$ and the nucleon density is $2.2\rho_0$: The Δ contribution is 20% in the test volume which contains, as a matter of fact, only 2.5 resonances. The total multiplicity of Δ resonances is just about 10% of the total nucleon multiplicity.

However, it is obvious that the other Δ's can be distributed all over the reaction volume. Figure 3(b) shows the Δ density distribution as experienced by the Δ's in the system at 5, 10, and 20 fm/c. The densities were calculated by summing over all contributing Gaussians of all Δ's in the system at the locations of the respective Δ's. We would like to point out that the mean Δ density experienced by the Δ's is about $0.25\rho_0$. Less than 1% of the Δ's experience Δ densities around $0.5\rho_0$. However, enough Δ's are in the system to show signs of collec-

tivity such as *collective flow* in the reaction plane. Its measurable signature [the pion $\vec{p_x}(y)$ distribution in central collisions] will be discussed in one of the following sections.

IV. INCLUSIVE PION OBSERVABLES

This section deals with inclusive pion production in relativistic heavy-ion collisions. Figure 4 shows the predicted impact parameter dependence of the multi-

FIG. 3. Time evolution of the the total baryon, nucleon, and Δ resonance density in units of ρ/ρ_0 (a) and Δ density distribution the respective Δ's experience for 5, 10, and 20 fm/c. The densities in the upper frame (a) are calculated in a sphere of 2 fm radius around the collision center. The hot and dense reaction phase lies between 5 and 20 fm/c during which approximately 10% of the nucleons are excited to Δ resonances. Up to 50% nuclear matter ground state density is reached by the Δ resonances. However, less than 1% of the Δ's experience such high densities. The average Δ density which is *felt* by the Δ's is approximately $0.25\rho_0$ at 10 fm/c. The densities in the lower frame (b) were calculated by summing over all contributing Gaussians of all Δ's in the system at the locations of the respective Δ's.
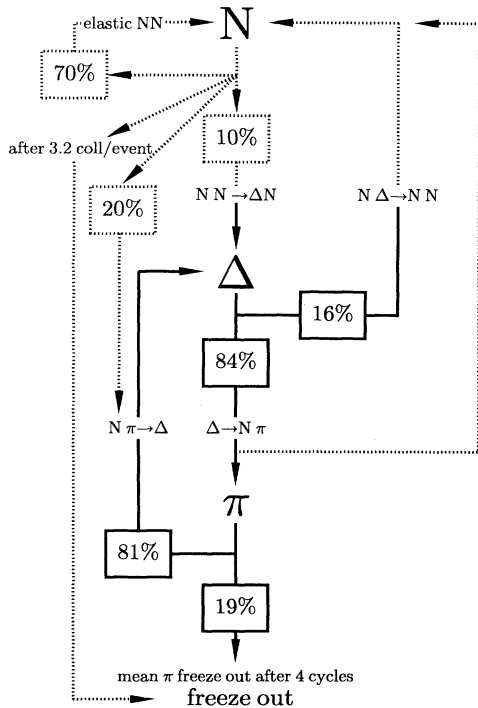

FIG. 2. Pion-nucleon cycle in the IQMD model. The scheme describes (for $b \leq 5$ fm and time averaged) all possible processes in the model linked to the creation of Δ matter. The probabilities in the boxes always refer to the vertices they are directly connected with. The main process for sustaining Δ matter is the $\Delta \to N\pi \to \Delta$ loop, which, however, first has to be fueled by the $NN \to \Delta N$ process.
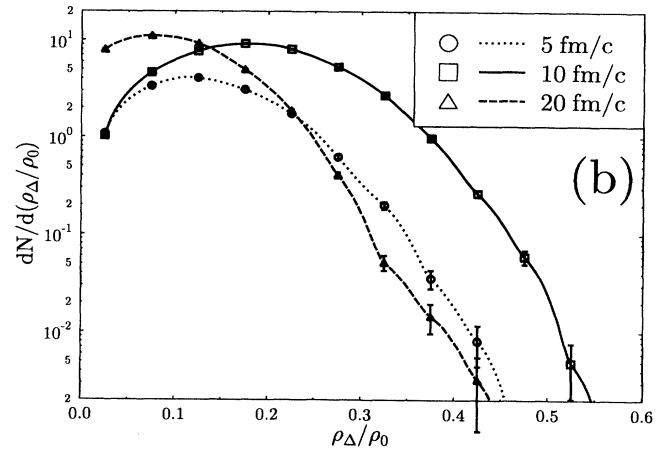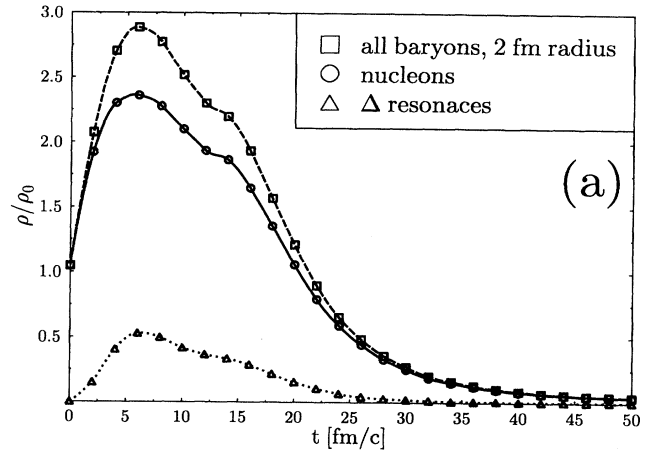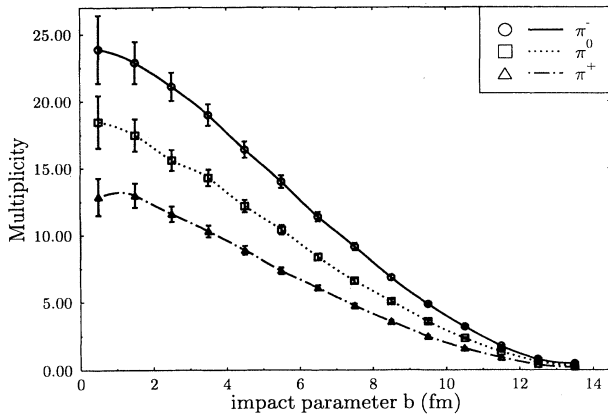
FIG. 4. Multiplicity of π^-, π^0, and π^+ versus impact parameter b for Au+Au collisions at 1 GeV/nucleon incident beam energy. A hard EOS with a momentum-dependent interaction is used. For central collisions ($b = 0$ fm) the total pion multiplicity is approximately 55. For a minimum bias impact parameter distribution the average pion multiplicity is about 19 (8 π^-, 6 π^0, and 5 π^+).

The polar angular distribution $\frac{dN}{d\cos\vartheta_{c.m.}}$ for π^-, π^0, and π^+ is shown in Fig. 6 for minimum bias events (a) and for π^- in central vs minimum bias events in (b). A horizontally flat distribution would correspond to isotropic emission. For minimum bias events (top) a strong peaking towards forward-backward angles is observed, most prominently for π^-.

This is important for the extrapolation of total yields from spectra measured at $\vartheta_{c.m.} = 90°$ — if the midrapidity spectra are used to extrapolate (with the assumption of a flat distribution), the total yield may be underestimated by a factor of 2. The anisotropy decreases when studying central collisions (bottom). This dependence can be explained by the decay of Δ resonances in the projectile- and target-spectator regions. The difference betweeen the distributions of π^- and π^+ also results in a forward-backward peaking of the N_{π^-}/N_{π^+} ratio. This phenomenon has already been experimentally observed for light collision systems at the BEVALAC [64].

Figure 7 shows a comparison of inclusive π^0 spectra for Au+Au and Ca+Ca (minimum bias and $y_{c.m.} \pm 0.16$) between the IQMD model and data published by the TAPS

plicity of π^-, π^0, and π^+ for Au+Au collisions at 1 GeV/nucleon incident beam energy. A hard EOS with a momentum-dependent interaction is used in the calculation. For central collisions ($b = 0$ fm) the total pion multiplicity is approximately 55. However, the average pion multiplicity is about 19 (8 π^-, 6 π^0, and 5 π^+) for a minimum bias impact parameter distribution.

The mass dependence of the total pion multiplicity is shown in Fig. 5. For light collision systems the multiplicity increases linearly with the system mass. However, for heavier systems the increase is less than the linear extrapolation; this is due to pion absorption. The values are for $b = 0$ fm calculations of the systems ^{20}Ne+^{20}Ne, ^{40}Ca+^{40}Ca, ^{58}Ni+^{58}Ni, ^{93}Nb+^{93}Nb, and ^{197}Au+^{197}Au.
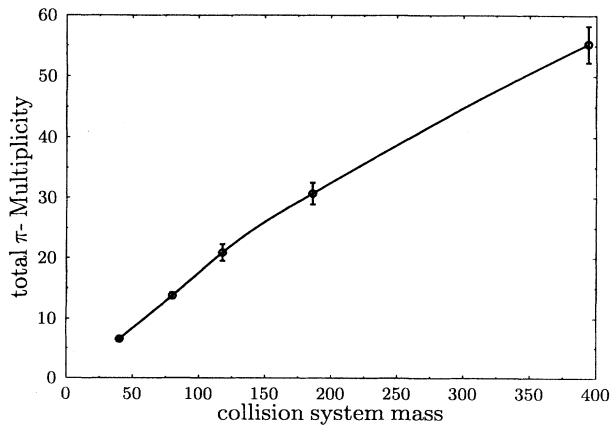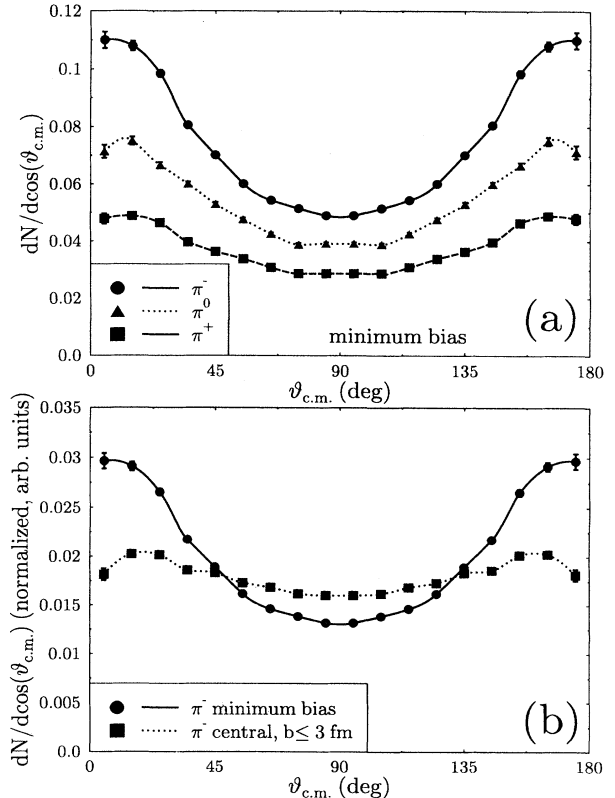

FIG. 5. Total pion multiplicity versus collision system mass at 1 GeV/nucleon beam energy. For light collision systems the multiplicity increases linearly with the system mass. However, for heavy systems the increase is less than linear due to pion absorption. The values plotted were extracted from $b = 0$ fm calculations of the systems Ne+Ne, Ca+Ca, Ni+Ni, Nb+Nb, and Au+Au.

FIG. 6. Polar angular distribution $\frac{dN}{d\cos\vartheta_{c.m.}}$ for π^-, π^0, and π^+ in minimum bias (a) and for π^- in minimum bias and central (b) Au+Au collisions. A horizontally flat distribution would correspond to an isotropic emission. For minimum bias events (top) a strong peaking towards forward-backward angles is observed, most prominently for π^-. The anisotropy decreases when studying central collisions (bottom). It can be explained by the decay of Δ resonances in the projectile- and target-spectator regions.
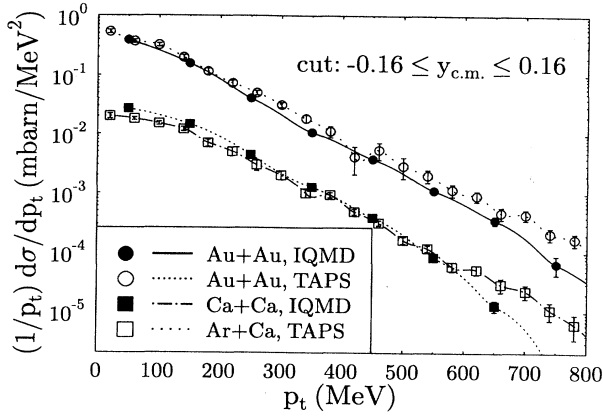
FIG. 7. Comparison of inclusive π^0 spectra $\frac{d\sigma}{p_t dp_t}$ for Au+Au and Ca+Ca (minimum bias) collisions between the IQMD model and data measured by the TAPS Collaboration. A hard EOS including momentum dependence is used and a rapidity cut according to the acceptance of the TAPS spectrometer is employed. The model shows reasonable agreement with the heavy system Au+Au but it overpredicts the π^0 yield of the light system Ca+Ca by approximately 60%. The yield of low-p_t pions in the heavy system is underpredicted by 10%.

FIG. 8. Inclusive π^- and π^+ spectra $\frac{d\sigma}{p_t dp_t}$ for Au+Au (minimum bias) collisions at 1 GeV/nucleon as calculated with the IQMD model and a π^+ spectrum measured by the KaoS Collaboration. A hard EOS including momentum dependence is used in the IQMD calculation and a rapidity cut according to the acceptance of the TAPS spectrometer is employed; the KaoS measurement has been acceptance corrected. The slope of the π^+ spectrum in the model calculation agrees well with the KaoS measurements. However, the multiplicity as predicted by the model is approximately 20% above the KaoS measurements.

Collaboration [65]. Whereas the model shows reasonable agreement with the heavy system Au+Au it overpredicts the π^0 yield of the light system Ca+Ca by approximately 60%. The charged pions (for Au+Au collisions) are shown in Fig. 8 together with π^+ data from the KaoS Collaboration [66]. The slope of the π^+ spectrum in the model calculation agrees well with the KaoS measurements. However, the multiplicity as predicted by the model is approximately 20% above the KaoS measurements. Both the calculation and the measurements have been acceptance corrected to the rapidity interval $y_{c.m.} \pm 0.16$ and may directly be compared to Fig. 7. Especially the measurement of high-energy pions is of great interest. They correlate directly to early freeze-out times and heavy Δ resonances [67].

The mass dependence of pion production and its sensitivity towards the transverse momentum p_t can be studied more clearly by plotting the ratio of the p_t spectra for Au+Au and Ca+Ca versus the transverse momentum p_t (Fig. 9). A comparison between data from the TAPS Collaboration [65] and the IQMD model is shown in Fig. 9. The model underpredicts this ratio by approximately a factor of 2, in particular for low transverse momenta. However, this holds for all transport model calculations which have been compared to the TAPS data [65]. A previous comparison between the IQMD model and the TAPS data in Ref. [65] showed far larger disagreement between model and data. This was due to an improper normalization of the theoretical calculations.

The yield of low-p_t pions in the heavy system is underpredicted by 10%. This is a common problem of most transport theories dealing with heavy-ion collisions. Suggested explanations for this underprediction include in-medium effects of pions in nuclear matter [57] and the neglect of Bose enhancement due to the bosonic nature
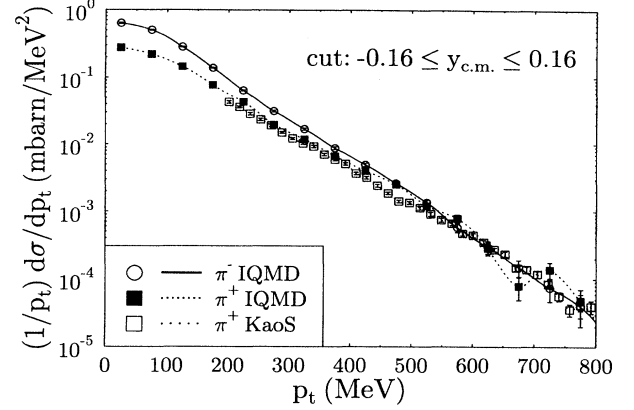
of the pions.

The importance of the inclusion of Coulomb forces and energy dependent π-N cross sections can be shown by plotting the π^- to π^+ ratio versus the transverse momentum p_t (Fig. 10). The solid line shows the full calculation including Coulomb forces. For high p_t the π^-/π^+ ratio decreases towards 1, whereas for low p_t it increases to 2.5 — considerably higher than the value of 1.8 predicted by the Δ-isobar model. The dashed line shows a calculation without Coulomb forces. This ratio remains constant at
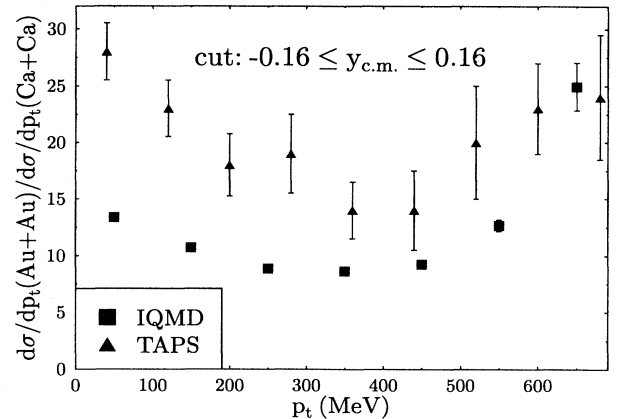

FIG. 9. Ratio of the pion yield from Au+Au and Ca+Ca collisions plotted versus the transverse momentum p_t. The figure shows a comparison between data measured by the TAPS Collaboration and an IQMD calculation (minimum bias, hard equation of state with momentum dependence). For low transvere momenta the model underpredicts the data approximately by a factor of 2.
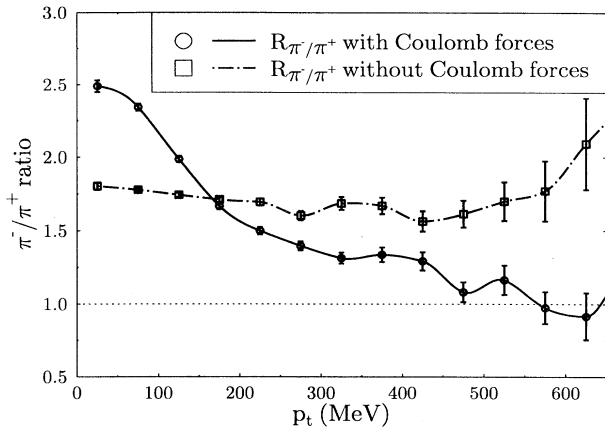
FIG. 10. π^- to π^+ ratio versus transverse momentum p_t for Au+Au collisions (minimum bias) at 1 GeV/nucleon with a hard EOS and momentum dependence. The solid line shows the full calculation including Coulomb forces. For high p_t the ratio decreases towards 1 whereas for low p_t it increases to 2.5, considerably higher than the value of 1.8 which the Δ-isobar model would suggest. The dashed line shows a calculation without Coulomb forces acting upon the pions. Within the error bars the ratio remains constant at a value around 1.8.

1.8. The (small) remaining variations might be due to the different energy dependence of the π^+ -p and π^- - p inelastic cross sections.

V. PION NUCLEON CORRELATION IN THE EVENT PLANE

The hydrodynamical model predicts a bounce-off of nuclear matter in the reaction plane [8,68] which has experimentally indeed been discovered [69,70]. The bounce-off is depicted by plotting the in-plane transverse momentum $\vec{p_x}(y)$ versus the rapidity y. For nucleons and light fragments a horizontal s shape is typically seen with negative $\vec{p_x}(y)$ values for $y \leq y_{c.m.}$ and positive $\vec{p_x}(y)$ values for $y \geq y_{c.m.}$. Figure 11 shows the $\vec{p_x}(y)$ distribution for π^+ and protons in Au(1A GeV)Au collisions with a minimum bias impact parameter distribution. The protons show the expected collective flow [71–73]. The $\vec{p_x}$ of the pions, however, is anticorrelated to that of the protons. A similar proton-π anticorrelation has been measured for the asymmetric system Ne+Pb at 800 MeV/nucleon by the DIOGENE Collaboration [74]. Transport model comparisons to the DIOGENE data with the IQMD [24] and the BUU [25] models have shown good agreement with the data.

We have studied the origin of the particular shape of the pion angular distribution and the $\vec{p_x}$ spectrum by sequentially suppressing first the *soft-delta* production and then the delta absorption (while allowing the soft-delta production). If we deactivate the soft-delta production (see Fig. 3), $\pi N \rightarrow \Delta$, pions are neither scattered nor absorbed after the initial production. No $\vec{p_x}$ for pions is observed. In order to decide whether the $\vec{p_x}$ spectrum is caused by absorption or by scattering we now deacti-
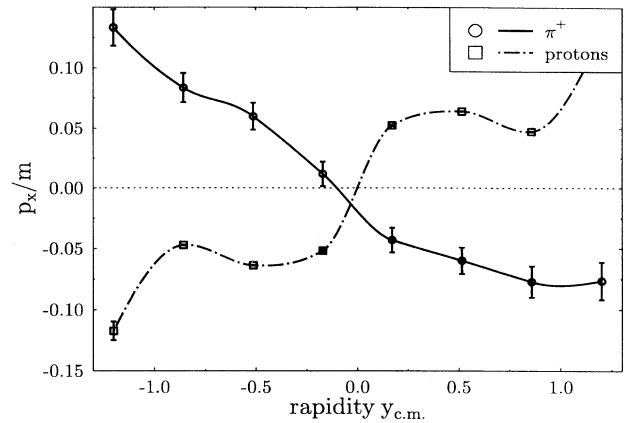

FIG. 11. Rapidity y vs $\vec{p_x}/m$ for π^+ and protons in Au+Au collisions at 1 GeV/nucleon with minimum bias impact parameter distribution and a hard EOS including momentum dependence. The protons show the expected bounce-off. The $\vec{p_x}$ of the pions is directed oppositely to that of the protons. This effect is caused by rescattering of pions from large chunks of spectator matter.

vate the reaction $\Delta N \rightarrow N N$. We thus suppress pion absorption but allow scattering — the anticorrelation between pions and protons in the $\vec{p_x}$ returns. In contrast to previous publications, which investigated the asymmetric system Ne(800A MeV)Pb and suggested the anticorrelation of pionic and nucleonic $\vec{p_x}$ at target rapidities to be caused by pion absorption [25], our investigation reveals the $\vec{p_x}$ spectrum of the pions to be dominated by the pion scattering process [26].

The following simplified picture can explain the origin of the observed phase space distribution: The Δ decays isotropically in its rest frame; therefore, 50% of the pions are emitted with a positive p_x and 50% with a negative p_x. At target rapidity those pions which obtain a positive p_x value usually do not have the chance to rescatter: Most of the target nucleons are located in the *negative* p_x area. Those pions which *do* rescatter at target rapidity are the ones with an initially *negative* p_x: Every time a Δ decays (isotropically) there is a 50% chance that this pion is emitted *upward*, i.e., into an azimuthal angle between $-90° \leq \phi \leq 90°$. These ϕ values characterize the hemisphere of positive p_x, by definition. This leads, for $\approx 50\%$ of the pions with, originally, negative p_x, to a shift towards a positive p_x. This remains true even after transforming back into the laboratory frame. The same consideration applies vice versa for projectile rapidity: Most projectile nucleons are located in the *positive p_x* area. The pions are rescattered in this area which results in a negative $\vec{p_x}$ and a maximum in the azimuthal angular distribution in the $90° \leq \phi \leq 270°$ interval.

Figure 12 shows the in-plane transverse momentum $\vec{p_x}$ versus rapidity y (in the c.m. system) for π^+ in central collisions of Au+Au (with impact parameters $b \leq 3$ fm). In contrast to (semi)peripheral collisions, however, $\vec{p_x}$ is correlated for pions and nucleons in central collisions because of the bounce-off of Δ resonances [75]. The square markers in Fig. 12 depict a calculation with the
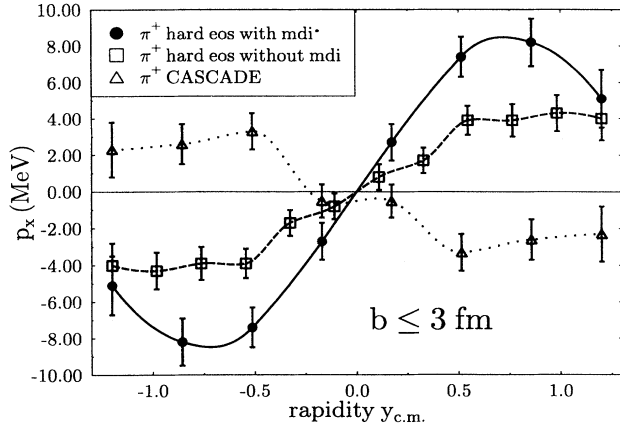
FIG. 12. In-plane transverse momentum $\vec{p_x}$ versus rapidity y (in the c.m. system) for π^+ in central Au+Au collisions with impact parameters $b \leq 3$ fm. Calculations with a hard equation of state without momentum dependence (squares), the same equation of state with momentum dependence (circles), and a CASCADE calculation (triangles) are shown. The effect of the momentum dependence is considerable, exhibiting the sensitivity of $\vec{p_x}$ on the baryon flow. The CASCADE calculation gives a different phase space distribution due to its lack of collective baryon flow.

hard equation of state without momentum dependence, and the circles show the same equation of state including momentum dependence, whereas the triangles represent a CASCADE calculation, i.e., a nonequilibrium free gas.

The momentum dependence enhances the $\vec{p_x}$ of the pions. This effect is due to the bounce-off of the Δ resonances [75] which in our model is enhanced because the momentum dependence for the Δ resonances is included in the same way as for the nucleons.

The CASCADE calculation, however, shows the opposite behavior. The $\vec{p_x}$ of the pions has a negative sign to that of the calculations with the density-dependent equations of state. This behavior can be explained by the lack of hadron collective flow in CASCADE calculations [76]. The pions would then be expected to be emitted isotropically $[\vec{p_x}(Y) = 0]$. However, pion scattering from small caps of spectator matter being present at impact parameters around 3 fm causes the observed anticorrelation [26]. In order to investigate the density dependence of the nuclear equation of state and in order to show the differences between CASCADE calculations and calculations including the equation of state more clearly we use the robust observable p_x^{dir} which for nucleons is defined as

$$p_x^{\text{dir}} = \frac{\displaystyle\sum_{i=1}^{A_P+A_T} p_x^i \text{sgn}(y_i - y_{\text{c.m.}})}{A_T + A_P}$$

(the adaptation for pions is straightforward) and plot it versus the impact parameter (Fig. 13). For positive values of p_x^{dir} the pion $\vec{p_x}$ vs rapidity distribution is correlated to that of the nucleons. For negative values an anticorrelation is observed.

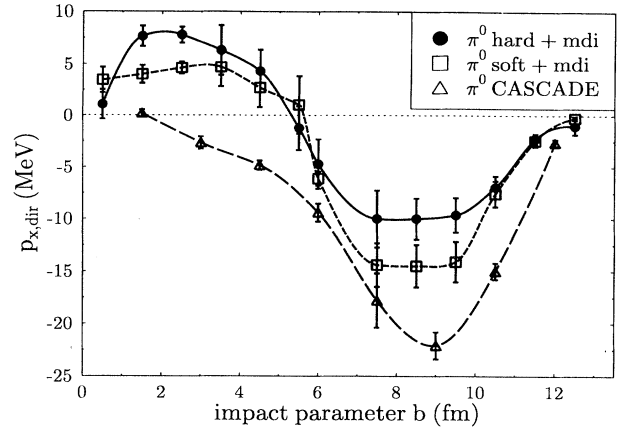Figure 13 shows the respective calculations for the hard

FIG. 13. p_x^{dir} versus impact parameter b for Au+Au collisions at 1 GeV/nucleon with hard and soft equations of state, both with momentum dependence, and for the CASCADE calculation. Note the clear sensitivity for the equation of state on p_x^{dir}. The CASCADE calculation exhibits an anticorrelation between pions and nucleons for the whole impact parameter range, due to pion nucleon scattering and its lack of collective baryon flow.

and soft equations of state (including momentum dependence) and for the CASCADE calculation. For small impact parameters the calculations with equation of state show a correlation between pion and nucleon bounce-off. At semiperipheral impact parameters we observe a sign reversal. As mentioned above, the anticorrelation between nucleon and pion bounce-off is caused by pion scattering in spectator matter [26]. In contrast, the CASCADE calculation exhibits a negative p_x^{dir} for the whole impact parameter range. The momentum transfer p_x^{dir} shows a systematic difference between the hard and soft equations of state. However, very high statistics and high-precision impact parameter classification are necessary to experimentally exploit this sensitivity towards the determination of the nuclear equation of state. The results of Figs. 11 and 13 show clearly that even in the domain of particle production $(\pi, K, \eta, \bar{p}, \rho, \omega)$ CASCADE simulations predict distinctly different phase space distributions for baryons and mesons at central impact parameters.

VI. AZIMUTHAL CORRELATIONS OF PIONS PEPENDICULAR TO THE EVENT PLANE

Now let us investigate particle emission perpendicular to the reaction plane. The hydrodynamical model predicted a squeeze-out of high-energetic nucleons perpendicular to the reaction plane [9,4,77]. This effect, which has also been predicted by QMD calculations [24,78–81] and has been confirmed by experiment [82–84], is due to the high compression of nuclear matter in the central hot and dense reaction zone (it is a genuinely collective effect, increasing linearly with A).

Do pions show a similar behavior? The azimuthal (φ) distribution of the pions is plotted to investigate this question. φ is the angle between the transverse momen-

tum vector $\vec{p_t}$ and the x axis (which lies in the reaction plane and is perpendicular to the beam axis). Thus $\varphi = 0°$ denotes the projectile hemisphere and $\varphi = 180°$ corresponds to the target hemisphere.

Figure 14 shows the respective distributions for neutral pions in the transverse momentum bins $p_t \leq 50$ MeV and $p_t \geq 400$ MeV at a minimum bias impact parameter distribution. The distributions have been normalized in order to fit into the same figure. The analysis was performed from $0°$ to $180°$ and then symmetrized for $180°$ to $360°$. The plotted distributions have been extracted by fitting the calculated points (shown for the high-p_t bin) according to the function $a[1 + b \cos(\phi) + c \cos(2\phi)]$. The azimuthal angular distribution for π^0 with low p_t shows maxima at $\varphi = 0°$ and $\varphi = 180°$ corresponding to a preferential emission in the reaction plane. The high-p_t π^0, however, show a maximum at $\varphi = 90°$. This maximum is associated with preferential particle emission perpendicular to the reaction plane. The inset shows data from the TAPS Collaboration [30] for the region 400 MeV $\leq p_t \leq$ 600 MeV and midrapidity. We observe a good qualitative agreement between the theoretical prediction and the experiment. It should be noted, however, that both theory and experiment need much better statistics to allow a conclusive quantitative comparison.

The magnitude of the observed anisotropy and its dependence on impact parameter and transverse momentum are best studied by using the following ratio:
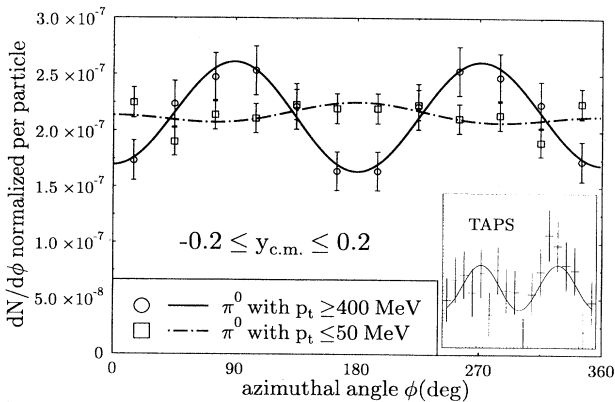
$$R_{\text{out/in}} = \left. \frac{\frac{dN}{d\varphi}(\varphi = 90°) + \frac{dN}{d\varphi}(\varphi = 270°)}{\frac{dN}{d\varphi}(\varphi = 0°) + \frac{dN}{d\varphi}(\varphi = 180°)} \right|_{y=y_{\text{c.m.}}}.$$

For positive $R_{\text{out/in}}$ values pions are emitted preferentially perpendicular to the reaction plane. Figure 15 shows the transverse momentum dependence of $R_{\text{out/in}}$ for Au+Au collisions with an impact parameters bewteen $b=5$ fm and $b=10$ fm and at midrapidity ($y_{\text{c.m.}} = \pm0.2$): In contrast to pions with low transverse momentum, which are emitted preferentially in the reaction plane, high-p_t pions are preferentially emitted perpendicular to the reaction plane. This effect is stronger for π^+ than for π^-. The difference is due to the different $\pi N \rightarrow \Delta$ production cross section for π^+ and π^- and due to Coulomb forces pushing the π^+ away from the spectator matter which is located mostly in the reaction plane. The π^-, on the other hand, are being attracted by those spectator-protons. These effects decrease the number of π^- leaving the reaction zone in a direction perpendicular to the reaction plane. However, the statistics accumulated so far are not large enough for a more detailed study of the differences between positive and negative pions. The inset of Fig. 15 shows recent measurements from the KaoS Collaboration [29] which confirm the predicted systematics of the p_t dependence. Imposing the limited acceptance of the KaoS spectrometer on the IQMD calculations would reduce the available statistics by one order of magnitude. Experimental uncertainties in the determination of the proper reaction plane result in a reduction of the measured $R_{\text{out/in}}$ values which are difficult to compensate. Therefore a direct quantitative comparison between the KaoS measurements and IQMD calculations is not feasable at this point of time.
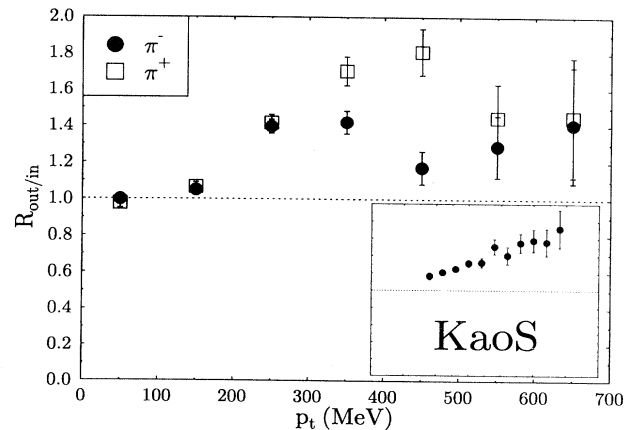
We have investigated the cause of the observed prefer-

FIG. 14. Normalized azimuthal angular distribution $dN/d\varphi$ for π^0 with low and high transverse momentum p_t at midrapidity in the reaction Au($1A$ GeV)Au with minimum bias impact parameter distribution, a hard equation of state, and momentum-dependent interaction. The points were fitted according to the function $a[1 + b \cos(\phi) + c \cos(2\phi)]$. The maximum at $\varphi = 90°$ corresponds to a preferential emission of high-p_t pions perpendicular to the reaction plane. This is due to pion absorption by large pieces of baryonic spectator matter located predominantly in the reaction plane. Perpendicular to the plane there is no such spectator matter and pions with high p_t can leave the reaction zone without further interaction. Low-p_t pions have rescattered more often which is only possible in the reaction plane. The inset shows data from the TAPS Collaboration for the region 400 MeV $\leq p_t \leq$ 600 MeV and midrapidity.

FIG. 15. Squeeze-out ratio $R_{\text{out/in}}$ versus transverse momentum p_t for π^+ and π^-. Pions with $p_t \geq 200$ MeV are preferentially emitted perpendicular to the reaction plane. Pions with $p_t \leq 100$ MeV are emitted isotropically because they have undergone frequent rescattering which can only happen due to spectator matter in the reaction plane. The differences between π^- and π^+ are due to Coulomb forces. The inset shows data on π^+ from the KaoS Collaboration (identical axis scaling).

ential emission perpendicular to the reaction plane: Pion absorption as well as scattering can be eliminated by deactivating the reaction $\pi N \to \Delta$; then, no squeeze-out is observed.

In order to decide whether the anisotropy is caused by absorption or by scattering the reaction $\Delta N \to N N$ can be deactivated. Thus pion absorption is suppressed but scattering is allowed: No anisotropy is observed. Therefore we conclude that the anisotropy is dominated by the pion absorption process [28].

Figure 16 shows the distribution of the number of delta generations n_Δ a pion goes through before its freeze-out. Here n_Δ is shown for π^+ emitted both in the reaction plane as well as perpendicular to it. $(n_\Delta - 1)$ is therefore the number of times a pion scatters before freeze-out. We observe that 90% of the produced pions scatter at least once before leaving the reaction zone. A large number of pions scatters even more often, 2% up to 10 times. The observed preferential emission perpendicular to the reaction plane is due to an excess of high-p_t pions which on the average have undergone fewer collisions (≤ 2) than the pions in plane. Those pions which make this effect do rescatter rarely; they are emitted early but carry information on the high-density phase of the reaction. They stem from the decay of the most massive delta resonances which are mostly produced early on in the reaction [67]. Therefore high-p_t pions emitted perpendicular to the event plane should be the most sensitive pionic probes for the investigation of the hot and early reaction zone.

Figure 17 shows the azimuthal angular distribution of high-p_t ($p_t \geq 400$ MeV) neutral pions at midrapidity and impact parameter $b{=}6$ fm. The different curves show calculations for hard (circles) and soft (squares) equations of state (including momentum dependence) and a CASCADE calculation (triangles). φ is the angle between the transverse momentum vector $\vec{p}_t$ and the x axis (which
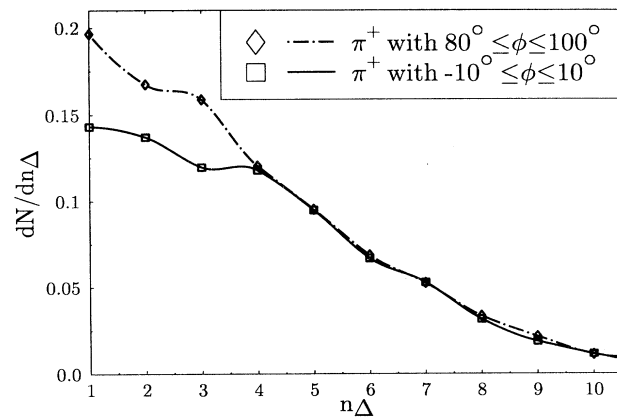

FIG. 16. Distribution of the number of delta generations n_Δ a pion goes through before its freeze-out for π^+ emitted in the reaction plane and perpendicular to it. 90% of the produced pions scatter at least once before leaving the reaction zone. The observed preferential emission perpendicular to the reaction plane is due to an excess of pions which on the average have undergone fewer collisions (≤ 2) than the pions in plane.
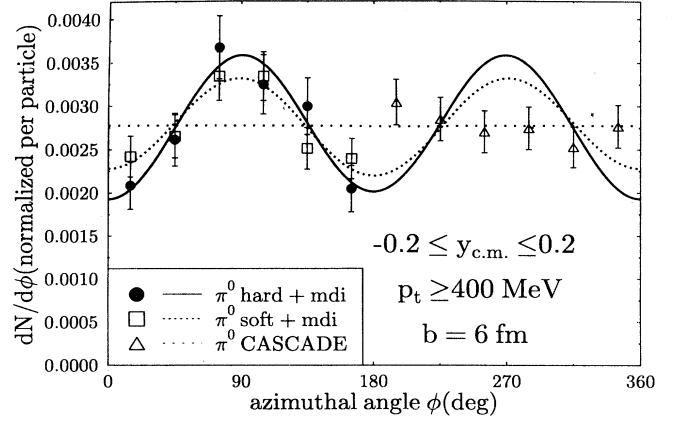

FIG. 17. Azimuthal angular distribution $dN/d\varphi$ for neutral pions calculated with hard and soft equations of state (both with momentum dependence) and a CASCADE calculation. All calculations were performed with an impact parameter of $b = 6$ fm. Both equations of state exhibit approximately the same angular distribution whereas the CASCADE calculation does not exhibit any peak perpendicular to the event plane. For larger impact parameters, however, also the CASCADE calculation shows a pronounced squeeze-out.

lies in the reaction plane and is perpendicular to the beam axis). The out-of-plane pion squeeze-out is clearly seen by the pronounced maximum at $\varphi = 90°$ for both equations of state. To enhance the statistics all particles are projected into the $0° \leq \varphi \leq 180°$ hemisphere. The solid and dashed lines are least squares fits with the function $f(\varphi) = a[1 + s_1 \cos(\varphi) + s_2 \cos(2\varphi)]$ which has been used to fit the squeeze-out phenomenon [82,83]. The curves show an extrapolation to the full azimuthal angular range. The distributions are normalized per particle in order subtract the influence of different equations of state on the pion multiplicity. Within error bars both equations of state exhibit the same out-of-plane pion squeeze-out. There is a trend for the hard equation of state to exhibit an enhanced out-of-plane pion squeeze-out but this trend might be too small to be useful for an experimental distinction between the different equations of state, whereas, in contrast, the in-plane pion bounce-off shows a clear difference for the two cases (see above). The CASCADE calculation does not exhibit any significant out-of-plane pion squeeze-out for $b{=}6$ fm. However, for larger impact parameters also CASCADE calculations exhibit a pronounced out-of-plane pion squeeze-out (Fig. 18).

Figure 18 shows $R_{\mathrm{out/in}}$ versus impact parameter b for the hard equation of state with and without momentum dependence of the real part of the nucleon optical potential. The momentum dependence causes a drastic increase of $R_{\mathrm{out/in}}$ for impact parameters larger than 3 fm. In the CASCADE calculation the onset of the out-of-plane pion squeeze-out is shifted toward larger impact parameters as compared to the calculations including the equation of state (see also Fig. 17). For peripheral collisions $R_{\mathrm{out/in}}$ reaches the same magnitude for the CASCADE calculation and the hard equation of state without momentum dependence.
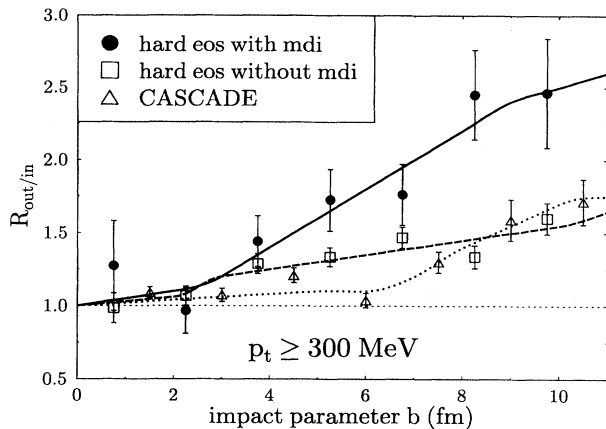
FIG. 18. *Squeeze-out ratio* $R_{out/in}$ versus impact parameter for neutral pions. The calculations were performed with the hard equation of state with (circles) and without (squares) momentum dependence as well as in CASCADE mode (triangles). Cuts around midrapidity $(-0.2 \leq y_{c.m.} \leq 0.2)$ and for high transverse momentum $(p_t \geq 300 \text{ MeV})$ were employed. For large impact parameters the CASCADE calculation agrees with the hard equation of state without momentum dependence. However, the onset of squeeze-out in CASCADE mode is shifted towards larger impact parameters in comparison with the hard equation of state. Most importantly, the inclusion of the momentum dependence results in a drastic increase of the squeeze-out ratio. The lines are inserted to guide the eye.

VII. CONCLUSION AND OUTLOOK

The physics responsible for the in-plane *pion* bounce-off (pion scattering) and the out-of-plane *pion* squeeze-out (pion absorption) differs completely from the compressional effects governing the in-plane *nucleon* bounce-off and out-of-plane *nucleon* squeeze-out. It is the pion-nucleon interaction which creates the sensitivity towards the density and momentum dependence of the nucleon optical potential. Therefore it is understandable that we observe a strong sensitivity towards the equation of state *in* the reaction plane whereas the sensitivity towards the equation of state *perpendicular* to the reaction plane is limited to the momentum dependence: The (anti)correlation in plane is caused by multiple pion nucleon scattering [26] with the bounced-off nucleons, which show a strong sensitvity towards momentum and density dependence [41]. The pion squeeze-out perpendicular to

the reaction plane, however, is dominated by high-p_t pions which have undergone less rescattering than those in the reaction plane [28]. The abundance of these high-p_t pions is correlated to the multiplicity of high-p_t nucleons which increases if the density dependence is included.

We have investigated the dependence of *pionic* in-plane bounce-off and out-of-plane squeeze-out on the *nuclear* equation of state. A strong sensitivity towards the *density dependence* is observed for the in-plane *pion* bounce-off whereas the out-of-plane *pion* squeeze-out shows only a small sensitivity. Both effects show a strong sensitivity toward the *momentum dependence*. CASCADE calculations, which we see as a crude approximation to QMD, give different phase space distributions for pions in both cases. It should be easy to resolve experimentally these two clearly qualitatively different distinct scenarios. The determination of the equation of state will require, on the other hand, a more sensitive (and sensible) quantitative comparison to theory, including an improved treatment of the Δ and pion optical potentials.

The nuclear equation of state cannot be extracted from one observable alone. All observables known to be sensitive to the equation of state have to be fitted simultaneously by the respective model in order to claim success. In this paper we have added additional, here *pionic*, observables which have to be taken into account for obtaining the final goal: The nuclear equation of state.

[1] W. Scheid, R. Ligensa, and W. Greiner, Phys. Rev. Lett. **21**, 1479 (1968).

[2] L. P. Csernai and J. I. Kapusta, Phys. Rep. **131**, 225 (1986).

[3] R. Stock, Phys. Rep. **135**, 261 (1986).

[4] H. Stöcker and W. Greiner, Phys. Rep. **137**, 277 (1986).

[5] R. B. Clare and D. Strottman, Phys. Rep. **141**, 179 (1986).

[6] B. Schürmann, W. Zwermann, and R. Malfliet, Phys. Rep. **147**, 3 (1986).

[7] W. Cassing, V. Metag, U. Mosel, and K. Niita, Phys. Rep. **188**, 365 (1986).

[8] H. Stöcker, J. A. Maruhn, and W. Greiner, Phys. Rev. Lett. **44**, 725 (1980).

[9] H. Stöcker, L. P. Csernai, G. Graebner, G. Buchwald, H. Kruse, R. Y. Cusson, J. A. Maruhn, and W. Greiner, Phys. Rev. C **25**, 1873 (1982).

[10] H. Stöcker, W. Greiner, and W. Scheid, Z. Phys. A **286**, 121 (1978).

[11] P. Danielewicz, Nucl. Phys. **A314**, 465 (1979).

[12] H. Stöcker, A. A. Ogloblin, and W. Greiner, Z. Phys. A **303**, 259 (1981).

[13] A. Sandoval, R. Stock, H. E. Stelzer, R. E. Renfordt, J. W. Harris, J. P. Brannigian, J. V. Geaga, L. J. Rosenberg, L. S. Schroeder, and K. L. Wolf, Phys. Rev. Lett. **45**, 874 (1980).

[14] R. Stock, R. Bock, R. Brockmann, J.W. Harris, A. Sandoval, H. Ströbele, K.L. Wolf, H.G. Pugh, L.S. Schroeder, M. Maier, R.E. Renfordt, A. Dacal, and M.E. Ortiz, Phys. Rev. Lett. **49**, 1236 (1982).

[15] J. Harris, R. Bock, R. Brockmann, A. Sandoval, R. Stock, H. Stroebele, G. Odyniec, L. Schroeder, R. E. Renfordt, D. Schall, D. Bangert, W. Rauch, and K. L. Wolf, Phys. Lett. **153B**, 377 (1985).

[16] S. Nagamiya, M.C. Lemaire, E. Moeller, S. Schnetzer, G. Shapiro, H. Steiner, and I. Tanihata, Phys. Rev. C **24**, 971 (1981).

[17] G.F. Bertsch, H. Kruse, and S. Das Gupta, Phys. Rev. C **29**, R673 (1984).

[18] H. Kruse, B. V. Jacak, and H. Stöcker, Phys. Rev. Lett. **54**, 289 (1985).

[19] A. Shor et al., Phys. Rev. Lett. **48**, 1597 (1982).

[20] J. Aichelin and C. M. Ko, Phys. Rev. Lett. **55**, 2661 (1985).

[21] J. Aichelin, A. Rosenhauer, G. Peilert, H. Stöcker, and W. Greiner, Phys. Rev. Lett. **58**, 1926 (1987).

[22] F. D. Berg and the TAPS Collaboration, Phys. Rev. Lett. **72**, 977 (1994).

[23] D. Miskowiec and the KaoS Collaboration Phys. Rev. Lett. **72**, 3650 (1994).

[24] Ch. Hartnack, H. Stöcker, and W. Greiner, in "Proceedings of the International Workshop on Gross Properties of Nuclei and Nuclear Excitation, XVI," Hirschegg, Kleinwalsertal, Austria, 1988, edited by H. Feldmeier (unpublished).

[25] B. A. Li, W. Bauer, and G. F. Bertsch, Phys. Rev. C **44**, 2095 (1991).

[26] S. A. Bass, C. Hartnack, R. Mattiello, H. Stöcker, and W. Greiner, Phys. Lett. B **302**, 381 (1993).

[27] M. Trzaska and the FOPI Collaboration, in "Proceedings of the XXXII Winter Meeting on Nuclear Physics," Bormio, Italy, 1994 (unpublished).

[28] S. A. Bass, C. Hartnack, H. Stöcker, and W. Greiner, Phys. Rev. Lett. **71**, 1144 (1993).

[29] D. Brill and the KaoS Collaboration, Phys. Rev. Lett. **71**, 336 (1993).

[30] L. Venema and the TAPS Collaboration, Phys. Rev. Lett. **71**, 835 (1993).

[31] J. J Molitoris and H. Stöcker, Phys. Rev. C **32**, R346 (1985).

[32] J. Aichelin and G. Bertsch, Phys. Rev. C **31**, 1730 (1985).

[33] E. A. Uehling and G. E. Uhlenbeck, Phys. Rev. **43**, 552 (1933); **44**, 917 (1934).

[34] C. Gregoire, B. Remaud, F. Sebille, L. Vinet, and Y. Raffray, Nucl. Phys. **A465**, 317 (1987).

[35] J. Aichelin and H. Stöcker, Phys. Lett. B **176**, 14 (1986).

[36] G. Peilert, H. Stöcker, A. Rosenhauer, A. Bohnet, J. Aichelin, and W. Greiner, Phys. Rev. C **39**, 1402 (1989).

[37] J. Aichelin, Phys. Rep. **202**, 233 (1991).

[38] H. Feldmeier, Nucl. Phys. **A515**, 147 (1990).

[39] A. Ono, H. Horiuchi, T. Maruyama, and A. Ohnishi, Phys. Rev. Lett. **68**, 2898 (1992).

[40] G. Peilert, J. Konopka, M. Blann, M. G. Mustafa,

[41] C. Hartnack, L. Zhuxia, L. Neise, G. Peilert, A. Rosenhauer, H. Sorge, J. Aichelin, H. Stöcker, and W. Greiner, Nucl. Phys. **A495**, 303 (1989).

[42] Ch. Hartnack, Ph.D. thesis, Univ. Frankfurt GSI Report No. 93-5, 1993.

[43] L. G. Arnold et al., Phys. Rev. C **25**, 936 (1982).

[44] G. Passatore, Nucl. Phys. **A95**, 694 (1967).

[45] G. F. Bertsch and S. Das Gupta, Phys. Rep. **160**, 189 (1988).

[46] G. Wolf, G. Batko, W. Cassing, U. Mosel, K. Niita, and M. Schäfer, Nucl. Phys. **A517**, 615 (1990).

[47] B. A. Li and W. Bauer, Phys. Lett. B **252**, 335 (1991); B. A. Li, W. Bauer, and G. F. Bertsch, Phys. Rev. C **44**, 450 (1991).

[48] Y. Yariv and Z. Frankel, Phys. Rev. C **20**, 2227 (1979).

[49] J. Cugnon, Phys. Rev. C **22**, 1885 (1980).

[50] A. Engel, W. Cassing, U. Mosel, M. Schäfer, and Gy. Wolf, Nucl. Phys. **A572**, 657 (1994).

[51] B. J. VerWest and R. A. Arndt, Phys. Rev. C **25**, 1979 (1982).

[52] P. Danielewicz and G. F. Bertsch, Nucl. Phys. **A533**, 712 (1991).

[53] J. Randrup, Nucl. Phys. **A314**, 429 (1979).

[54] J. Cugnon, T. Mizutani, and J. Vandermeulen, Nucl. Phys. **A352**, 505 (1981).

[55] S. Huber and J. Aichelin, Nucl. Phys. **A573**, 587 (1994).

[56] W. Ehehalt, W. Cassing, A. Engel, U. Mosel, and Gy. Wolf, Phys. Lett. B **298**, 31 (1993).

[57] L. Xiong, C. M. Ko, and V. Koch, Phys. Rev. C **47**, 788 (1993).

[58] G. F. Chapline, M. H. Johnson, E. Teller, and M. S. Weiss, Phys. Rev. D **8**, 4302 (1973).

[59] J. Boguta, Phys. Lett B **109**, 251 (1982); J. Boguta and H. Stöcker, ibid. **120**, 289 (1983).

[60] B. Waldhauser, J. A. Maruhn, H. Stöcker, and W. Greiner, Z. Phys. A **328**, 19 (1987).

[61] V. Metag, Prog. Part. Nucl. Phys. **30**, 75 (1993).

[62] W. Ehehalt, W. Cassing, A. Engel, U. Mosel, and G. Wolf, Phys. Rev. C **47**, R2467 (1993).

[63] M. Hofmann, R. Mattiello, N. S. Amelin, M. Berenguer, A. Dumitru, A. Jahns, A. v. Keitz, Y. Pürsün, T. Schönfeld, C. Spieles, L. A. Winckelmann, H. Sorge, J. A. Maruhn, H. Stöcker, and W. Greiner, Nucl. Phys. **A566**, 15c (1994).

[64] W. Benenson et al., Phys. Rev. Lett. **43**, 683 (1979).

[65] O. Schwalb and the TAPS Collaboration, Phys. Lett. B **321**, 20 (1994).

[66] Ch. Müntz and the KaoS Collaboration, Z. Phys. A (to be published).

[67] S. A. Bass, C. Hartnack, H. Stöcker, and W. Greiner, Phys. Rev. C **50**, 2167 (1994).

[68] H. Stöcker, J. A. Maruhn, and W. Greiner, Z. Phys. A **293**, 173 (1979).

[69] L. P. Csernai, W. Greiner, H. Stöcker, I. Tanihata, S. Nagamiya, and J. Knoll, Phys. Rev. C **25**, 2482 (1982).

[70] H. H. Gutbrod, A. M. Poskanzer, and H. G. Ritter, Rep. Prog. Phys. **52**, 1267 (1989).

[71] J. J. Molitoris and H. Stöcker, Phys. Lett. **162B**, 47 (1985).

[72] H.-A. Gustafsson, H. H. Gutbrod, B. Kolb, H. Löhner, B. Ludewigt, A. M. Poskanzer, T. Renner, H. Riedesel, H. G. Ritter, A. Warwick, F. Weik, and H. Wieman,

H. Stöcker, and W. Greiner, Phys. Rev. C **46**, 1457 (1992).

Phys. Rev. Lett. **52**, 1590 (1984).

[73] J. J. Molitoris, H. Stöcker, and B. L. Winer, Phys. Rev. C **36**, 220 (1986).

[74] J. Gosset, O. Vallette, J. P. Alard, J. Augerat, R. Babinet, N. Basid, F. Brochard, N. De Marco, P. Dupieux, Z. Fodor, L. Faysse, P. Gorodetzky, M. C. Lemaire, D. L'Hote, B. Lucas, J. Marroncle, G. Montarou, M. J. Parizet, J. Poitou, C. Racca, A. Rahmani, W. Schimmerling, and Y. Terrien, Phys. Rev. Lett. **62**, 1251 (1989); J. Poitou and the DIOGENE Collaboration, in "Proceedings of the International Workshop on Gross Properties of Nuclei and Nuclear Excitations XVI," Hirschegg, Kleinwalsertal, Austria, 1989 (unpublished).

[75] S. A. Bass, M. Hofmann, C. Hartnack, H. Stöcker, and W. Greiner, Phys. Lett. B **335**, 289 (1994).

[76] J. J. Molitoris, H. Stöcker, H. A. Gustafsson, J. Cugnon, and D. L'Hote, Phys. Rev. C **33**, 867 (1986).

[77] G. Buchwald, G. Gräbner, J. Theis, H. Stöcker, K. Frankel, M. Gyulassy, J. Maruhn, and W. Greiner,

[78] Ch. Hartnack, H. Stöcker, and W. Greiner, in *Proceedings of the NATO Advanced Study Institute on the Nuclear Equation of State* (Peñiscola, Spain), edited by W. Greiner and H. Stöcker (Plenum, New York, 1990).

[79] Ch. Hartnack, M. Berenguer, A. Jahns, A.v. Keitz, R. Mattiello, A. Rosenhauer, J. Schaffner, Th. Schönfeld, H. Sorge, L. Winckelmann, H. Stöcker, and W. Greiner, Nucl. Phys. **A538**, 53c (1992).

[80] Ch. Hartnack, J. Aichelin, H. Stöcker, and W. Greiner, Mod. Phys. Lett. (to be published).

[81] S. A. Bass, C. Hartnack, H. Stöcker, and W. Greiner, GSI Report No. 94-12, Z. Phys. A (to be published).

[82] H. H. Gutbrod, K. H. Kampert, B. W. Kolb, A. M. Poskanzer, H. G. Ritter, and H. R. Schmidt, Phys. Lett. B **216**, 267 (1989).

[83] H. H. Gutbrod, A. M. Poskanzer, and H. G. Ritter, Rep. Prog. Phys. **52**, 1267 (1989).

[84] The LAND Collaboration, Y. Leifels *et al.*, Phys. Rev. Lett. **71**, 963 (1993).

Phys. Rev. C **28**, 2349 (1983).